CoMFA and CoMSIA Studies on 1,3-Bis(benzylidene)-3,4-dihydro-1*H*-naphthalen-2-one, 2,6-Bis(benzylidene)cyclohexanone, and 3,5-Bis(benzylidene)-4-piperidone Series of Cytotoxic Compounds

Maulik R. Patel,[†] Jonathan R. Dimmock,*[,‡] and Tanaji T. Talele*[,†]

Department of Pharmaceutical Sciences, College of Pharmacy and Allied Health Professions, St. John's University, Jamaica, New York 11439, and College of Pharmacy and Nutrition, University of Saskatchewan, 110 Science Place, Saskatoon, Saskatchewan, Canada S7N 5C9

Received June 14, 2007

A number of 1,3-bis(benzylidene)-3,4-dihydro-1*H*-naphthalen-2-ones, 2,6-bis(benzylidene)cyclohexanones, and 3,5-bis(benzylidene)-4-piperidones possess significant potencies toward L1210, Molt 4/C8, and CEM cell lines. The objective of the current 3D QSAR study is to discover some of the structural parameters which govern cytotoxic potencies. The CoMFA models with steric and electrostatic fields provided satisfactory statistical data [($r^2_{cv} = 0.485$, $r^2_{ncv} = 0.834$, $r^2_{pred} = 0.591$), ($r^2_{cv} = 0.532$, $r^2_{ncv} = 0.850$, $r^2_{pred} = 0.729$), and ($r^2_{cv} = 0.561$, $r^2_{ncv} = 0.864$, $r^2_{pred} = 0.666$)] in regard to the cytotoxic potencies observed toward L1210, Molt 4/C8, and CEM cell lines, respectively. The CoMSIA model with steric, electrostatic, hydrophobic, and H-bond donor fields exhibited $r^2_{cv} = 0.513$, $r^2_{ncv} = 0.833$, and $r^2_{pred} = 0.562$ for cytotoxic activity toward L1210 cells, while the best CoMSIA models were obtained by a combination of steric, electrostatic, and hydrophobic fields which yielded statistically significant data [($r^2_{cv} = 0.531$, $r^2_{ncv} = 0.828$, $r^2_{pred} = 0.652$) and ($r^2_{cv} = 0.560$, $r^2_{ncv} = 0.841$, $r^2_{pred} = 0.729$)] to explain the cytotoxicity toward Molt 4/C8 and CEM cells, respectively. The information obtained from the CoMFA and CoMSIA 3D contour maps can be used in the design of more potent cytotoxins.

INTRODUCTION

For a number of years, the principal research in one of our laboratories has been the design and synthesis of novel conjugated benzylidene ketones as candidate antineoplastic agents. The reasons for undertaking these studies include the following considerations. First, various investigations revealed that these compounds have a preferential or exclusive affinity for thiols in contrast to amino or hydroxy groups.[1−4] Since these latter two groups are found in nucleic acids, thiol alkylators may be bereft of the genotoxic properties of a number of anticancer drugs used today.[5] Second, thiol groups are present in a variety of cellular constituents, and the advantages of compounds which interfere with multiple molecular targets have been emphasized recently.[6−8] Evidence for these compounds being thiol alkylators was provided when compound **55** as the hydrochloride salt lowered murine hepatic thiol concentrations.[9] The fact that these compounds are pleiotropic was confirmed by several investigations which revealed the different modes of action of representative 1,5-diaryl-3-oxo-1,4-pentadienes. Thus two of these compounds induced apoptosis in human HL-60 promyelocytic leukemia cells and HSC-2 squamous cell carcinoma and activated caspases -3, -8, and -9.[10] In addition, apoptosis in human HepG2 liver cancer cells was observed by an *N*-acyl analog of a 3,5-bis(arylidene)-4-piperidone[11] and a substituted 1,3-bis(benzylidene)-3,4-dihydro-1*H*-naphthalen-2-one.[12] Various 3,5-bis(benzylidene)-4-piperidones and related compounds are potent stimulators of fyn kinase[13] and weakly inhibit human *N*-myristoyltranferase.[14] Third, support for a markedly divergent mode of action than contemporary anticancer drugs was obtained when tumors which were resistant to a number of anticancer drugs, including the alkylating agent melphalan, were virtually free from cross resistance to various Mannich bases of α,β-unsaturated ketones.[15] Fourth, the theory of sequential cytotoxicity was proposed by one of the current investigators which states that the successive release of two or more cytotoxic agents may be more detrimental to malignant cells than normal tissues.[16] The reasons for proposing this hypothesis include the observation that on occasions the lowering of the concentration of chemoprotectant thiols prior to the administration of an anticancer drug exerted a greater toxicity to malignant rather than normal cells.[17,18] Hence a number of the enones prepared in these laboratories incorporated the 1,5-diaryl-3-oxo-1,4-pentadienyl pharmacophore into the structures in order that successive thiolations could take place at the 1 and 5 olefinic carbon atoms. Fifth, many of the conjugated enones prepared were well tolerated in short-term toxicity studies in rodents. For example, doses up to and including 300 mg/kg of many of these compounds did not produce fatalities,[19,20] whereas the LD_{50} values of melphalan, chlorambucil, and mitomycin C are 21.7, 58.0. and 12.3 mg/kg, respectively.[21]

This study is the first time that an in depth evaluation of various structural parameters of these novel cytotoxins has

* Corresponding author phone: (718)-990-5405; fax: (718)-990-1877; e-mail: talelet@stjohns.edu (T.T.T.), phone: (306)-966-6331; fax: (306)-966-6377; e-mail: jr.dimmock@usask.ca (J.R.D.).
[†] St. John's University.
[‡] University of Saskatchewan.

10.1021/ci700210z CCC: $37.00
Published on Web 10/18/2007

been undertaken. In other words, in view of the perceived importance of conjugated benzylidene ketones as candidate cytotoxins and especially those containing the 1,5-diaryl-3-oxo-1,4-pentadienyl pharmacophore, the decision was made to rigorously examine a number of physicochemical parameters of representative molecules with a view to determining some of the parameters which govern cytotoxic potencies. Thus some of the biodata for the enones **1**−**62** were culled from the literature which describe their evaluation against murine L1210 lymphoid leukemic cells as well as human Molt 4/C8 and CEM T-lymphocytes.[19,20,22,23] The approach taken in this study was to use 3D QSAR methodologies, namely comparative molecular field analysis (CoMFA)[24,25] and comparative molecular similarity indices analysis (CoMSIA),[26] and the results of these investigations are now reported.

MATERIALS AND METHODS

Data Sets and Biological Activity. The training and test sets used in this study comprise a series of 1,3-bis-(benzylidene)-3,4-dihydro-1*H*-naphthalen-2-one,[19] 2,6-bis-(benzylidene)cyclohexanone,[20,22] and 3,5-bis(benzylidene)-4-piperidone[23] analogues. An attractive quality of these compounds is their relative conformational rigidity, which makes them more amenable to meaningful CoMFA and CoMSIA analyses than flexible molecules. Besides, X-ray crystallographic (XRC) data on representative compounds from each series have been determined in our laboratory that provided suitable templates for modeling the compounds in the present study.[19,22,23] The IC_{50} values in units of M were converted to pIC_{50} ($-\log IC_{50}$) in order to give numerically larger data values for the active compounds than those of the inactive compounds. The pIC_{50} values were used as dependent variables in CoMFA and CoMSIA QSAR analyses. As a rule of thumb, the pIC_{50} values of the training data set should span approximately 3 log units. Accordingly the pIC_{50} values of the training set for L1210, Molt 4/C8, and CEM cell lines described in this manuscript range from 3.62 to 6.38, 3.63 to 6.82, and 3.73 to 6.59, respectively. The compounds in the test set were selected to approximately represent the distribution of biological data and structural classes in the training set. Hence, the test set is a true representative of the training set. The mean (sd) of the biological activity (pIC_{50}) in the training set and the test set were 4.88 (0.58) and 4.87 (0.40) for the L1210 cell line; 5.13 (0.65) and 5.10 (0.60) for the Molt 4/C8 cell line; and 5.16 (0.61) and 5.09 (0.52) for the CEM cell line. The structures of the training and test sets of compounds are shown in Tables 1 and 2, respectively.

Molecular Modeling and Alignment. All computational studies were performed using a SYBYL version 7.2[27] on a Dell Precision 470n workstation with the RHEL 4.0 operating system. The molecular conformation and alignment of molecules are two sensitive input parameters affecting the CoMFA model. The 3D structures of the compounds in the training and test sets were constructed using the Sketch Molecule function in SYBYL. Energy minimizations were performed with the conjugate gradient method using the Tripos force field[28] and Gasteiger−Marsili charges[29] with a convergence criterion of 0.001 kcal/mol Å. Each structure was further subjected to simulated annealing as it enables the rapid identification of a reasonable conformation.[30] The system was heated at 1000 K for 1 ps and then cooled at 200 K for 1 ps. The exponential annealing function was used, and ten such cycles were run. Using this method, the conformer in the training and the test set compounds with the least energy content was identified and subsequently subjected to further minimization with the same criteria as mentioned above. The conformational energy obtained by the simulated annealing method for compound **60** was found to be 14.8 kcal/mol, whereas the corresponding energy of the X-ray crystallographic conformation of the same molecule was 72.11 kcal/mol. This discrepancy in conformational energy could be potentially due to crystal packing as there are multiple copies of the molecule that try to pack in 3D space. In XRC the molecule may assume an energetically unfavorable conformation state in its packing. Moreover, the simulated annealing was carried out in the gas phase to obtain the global minimum conformation and theoretically should not yield the same conformation obtained by the X-ray diffraction method. It was interesting to note that the X-ray structure conformation of compound **60** upon simulated annealing followed by energy minimization led to a conformation with 15.8 kcal/mol energy. Superimposition of these two conformations led to an rmsd value of 0.1 which suggests that these conformers are quite identical. These findings further support our choice for using the conformation obtained from simulated annealing followed by the energy minimization method rather than the one obtained from the X-ray diffraction method. Together, the conformation used for the 3D QSAR study is of lowest energy content compared to the one obtained by the X-ray diffraction method. These conformations were used for the alignment.

Since structural information on these inhibitor−protein complexes remains to be solved, the most potent compound **62** was chosen as a template to fit the rest of the training and the test set compounds by using the SYBYL fit atoms function. The reference atoms in compound **62** used for alignment were as follows: (i) N_1, C_2, C_3, and C_4 of the 4-piperidone ring; (ii) C_5 as well as C_6 and C_7 of the B ring; and (iii) $C_{5'}$ as well as $C_{6'}$ and $C_{7'}$ of the A ring (Figure 1A). The alignment of the training and the test set compounds is shown in Figure 1B.

CoMFA and CoMSIA 3D QSAR Models. In deriving the CoMFA and CoMSIA descriptor fields, a 3D cubic lattice with grid spacing of 2 Å in *x*, *y*, and *z* directions was created to encompass the aligned molecules. CoMFA descriptors were calculated using an sp^3 carbon probe atom with a van der Waals radius of 1.52 Å and a charge of +1.0 to generate steric (Lennard-Jones 6-12 potential) field energies and electrostatic (Coulombic potential) fields with a distance-dependent dielectric at each lattice point. The values of steric and electrostatic energies were truncated at 30 kcal/mol. The CoMFA steric and electrostatic fields thus generated were scaled by the CoMFA-STD method in SYBYL.

CoMSIA descriptors were derived according to Klebe et al.[26] with the same lattice box as that used for the CoMFA calculations, with a grid spacing of 2 Å and employing a C^{1+} probe atom with a radius of 1.0 Å as implemented in SYBYL. CoMSIA similarity indices (A_F) for a molecule

Table 1. Structures of 62 Cytotoxic Compounds Used as the Training Set

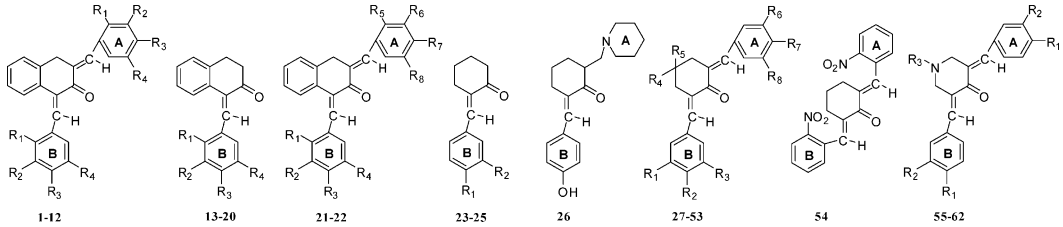

compd	R_1	R_2	R_3	R_4	R_5	R_6	R_7	R_8
1	H	H	H	H	-	-	-	-
2	H	H	Cl	H	-	-	-	-
3	H	H	F	H	-	-	-	-
4	H	F	H	F	-	-	-	-
5	H	H	OH	H	-	-	-	-
6	H	H	OCH_3	H	-	-	-	-
7	H	OCH_3	OCH_3	OCH_3	-	-	-	-
8	H	H	COO-allyl	H	-	-	-	-
9	NO_2	H	H	H	-	-	-	-
10	H	NO_2	H	H	-	-	-	-
11	H	NO_2	OH	H	-	-	-	-
12	H	H	$N(CH_3)_2$	H	-	-	-	-
13	H	H	H	H	-	-	-	-
14	H	Cl	Cl	H	-	-	-	-
15	H	H	CH_3	H	-	-	-	-
16	H	H	OCH_3	H	-	-	-	-
17	NO_2	H	H	H	-	-	-	-
18	H	H	NO_2	H	-	-	-	-
19	H	H	COOH	H	-	-	-	-
20	H	OCH_3	OCH_3	OCH_3	-	-	-	-
21	H	H	NO_2	H	H	OCH_3	OCH_3	OCH_3
22	H	OCH_3	OCH_3	OCH_3	H	H	NO_2	H
23	CH_3	H	-	-	-	-	-	-
24	OCH_3	H	-	-	-	-	-	-
25	OH	H	-	-	-	-	-	-
27	H	H	H	H	H	H	OH	H
28	H	Cl	H	H	H	H	OH	H
29	H	CH_3	H	H	H	H	OH	H
30	H	OCH_3	H	H	H	H	OH	H
31	H	OH	H	H	H	H	OH	H
32	H	H	H	H	H	H	OH	CH_2-piperidine
33	H	Cl	H	H	H	H	OH	CH_2-piperidine
34	H	OCH_3	H	H	H	H	OH	CH_2-piperidine
35	H	OH	$CH_2N(CH_3)_2$	H	H	H	OH	$CH_2N(CH_3)_2$
36	H	H	H	H	H	H	H	H
37	H	Cl	H	H	H	H	Cl	H
38	Cl	Cl	H	H	H	Cl	Cl	H
39	H	NO_2	H	H	H	H	NO_2	H
40	H	H	H	Br	H	H	H	H
41	H	Cl	H	Br	H	H	Cl	H
42	H	OCH_3	H	Br	H	H	OCH_3	H
43	H	CH_3	H	$C(CH_3)_3$	H	H	CH_3	H
44	H	OCH_3	H	$C(CH_3)_3$	H	H	OCH_3	H
45	H	F	H	$C(CH_3)_3$	H	H	F	H
46	H	Cl	H	$=CHCOOC_2H_5$		H	Cl	H
47	H	OCH_3	H	$=CHCOOC_2H_5$		H	OCH_3	H
48	H	F	H	$=CHCOOC_2H_5$		H	F	H
49	H	H	H	$-OCH_2CH_2O-$		H	H	H
50	H	NO_2	H	$-OCH_2CH_2O-$		H	NO_2	H
51	OCH_3	OCH_3	OCH_3	$-OCH_2CH_2O-$		OCH_3	OCH_3	OCH_3
52	H	H	H	$OCOCH_3$	H	H	H	H
53	H	CH_3	H	$OCOCH_3$	H	H	CH_3	H
55	H	H	H	-	-	-	-	-
56	Cl	H	H	-	-	-	-	-
57	F	H	H	-	-	-	-	-
58	$N(CH_3)_2$ H	H	-	-	-	-	-	
59	H	H	$COCH=CH_2$	-	-	-	-	-
60	Cl	H	$COCH=CH_2$	-	-	-	-	-
61	Cl	Cl	$COCH=CH_2$	-	-	-	-	-
62	NO_2	H	$COCH=CH_2$	-	-	-	-	-

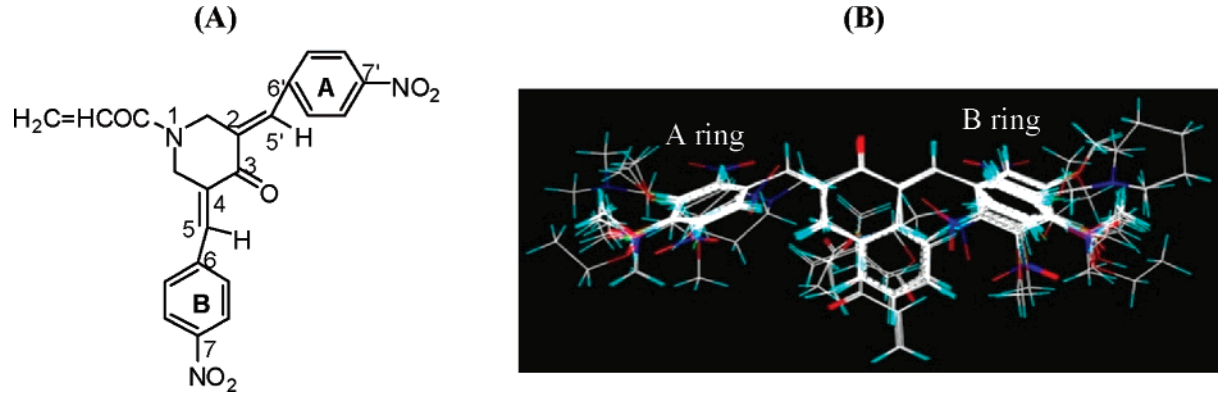

Figure 1. (A) Compound **62** used as a template for atom based alignment. The atoms for alignment are numbered. Note that the atom numbering does not follow IUPAC rules. (B) The training and test sets are aligned on the minimum energy conformation of compound **62**.

Table 2. Structures of Cytotoxic Compounds Used as the Test Set

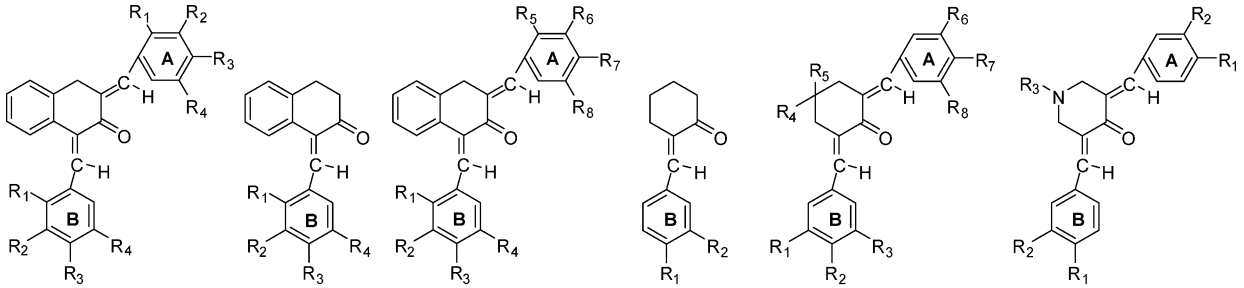

compd	R_1	R_2	R_3	R_4	R_5	R_6	R_7	R_8
63	H	H	Br	H	-	-	-	-
64	H	H	$OCOCH_3$	H	-	-	-	-
65	H	H	Cl	H	-	-	-	-
66	H	H	$N(CH_3)_2$	H	-	-	-	-
67	H	H	NO_2	H	H	H	Cl	H
68	H	H	-	-	-	-	-	-
69	H	Cl	Cl	H	H	H	OH	H
70	H	Cl	Cl	H	H	H	OH	CH_2-piperidine
71	H	F	H	H	H	H	F	H
72	H	F	H	Br	H	H	F	H
73	Cl	Cl	H	$C(CH_3)_3$	H	Cl	Cl	H
74	Cl	Cl	H	$=CHCOOC_2H_5$		Cl	Cl	H
75	Cl	Cl	H	$-OCH_2CH_2O-$		Cl	Cl	H
76	H	OCH_3	H	$-OCOCH_3$	H	H	OCH_3	H
77	NO_2	H	H	-	-	-	-	-
78	F	H	$COCH=CH_2$	-	-	-	-	-

j with atoms *i* at a grid point *q* were calculated using eq 1:

$$A_{F,k}{}^{q}(j) = -\sum \omega_{probe,k}\omega_{ik}e_{iq^2}{}^{-\alpha r} \qquad (1)$$

Being an extension to the CoMFA approach which has two fields, the CoMSIA method incorporates five different physicochemical properties (steric, electrostatic, hydrophobic, hydrogen bond donor, and hydrogen bond acceptor) denoted as *k* in eq 1, which were evaluated using the probe atom. A Gaussian type distance-dependence was used between the grid point *q* and each atom *i* in the molecule. A default value of 0.3 was used as the attenuation factor α. In CoMSIA, the steric indices are related to the third power of the atomic radii, the electrostatic descriptors are derived from partial atomic charges, the hydrophobic fields are derived from atom based parameters,[31] and the hydrogen-bond donor and acceptor atoms within a putative protein environment are derived from experimental values.[32,33]

The CoMFA and CoMSIA descriptors were used as independent variables, and the pIC_{50} values were used as dependent variables in PLS regression analyses[34,35] to derive 3D QSAR models using the standard implementation in the SYBYL package. The predictive value of the models was evaluated first by leave-one-out (LOO) cross-validation.[25,36] The cross-validated coefficient, q^2 (r^2_{cv}), was calculated using eq 2

$$r^2_{cv} = 1 - \frac{\sum(Y_{predicted} - Y_{observed})^2}{\sum(Y_{observed} - Y_{mean})^2} \qquad (2)$$

where $Y_{predicted}$, $Y_{observed}$, and Y_{mean} are predicted, actual, and mean values of the target property (pIC_{50}), respectively. Σ-

Table 3. Summary of CoMFA and CoMSIA Results

	CoMFA			CoMSIA		
PLS statistics	L1210 60 compds	Molt 4/C8 62 compds	CEM 62 compds	L1210 61 compds	Molt 4/C8 62 compds	CEM 62 compds
r^2 [a]	0.834	0.850	0.864	0.833	0.828	0.841
SEE[b]	0.245	0.261	0.236	0.247	0.279	0.254
F_{test}[c]	54.119	63.525	70.979	54.872	54.042	59.366
q^2 [d]	0.485	0.532	0.561	0.513	0.531	0.560
SEP[e]	0.505	0.548	0.514	0.492	0.541	0.503
r^2_{pred}[f]	0.591	0.729	0.666	0.562	0.652	0.729
PLS comp.[g]	5	5	5	5	5	5
contribution						
steric	0.55	0.59	0.58	0.20	0.28	0.28
electrostatic	0.45	0.41	0.42	0.31	0.36	0.34
hydrophobic	-	-	-	0.30	0.36	0.37
H-bond donor	-	-	-	0.19	-	-
r^2_{boot}[h]	0.874	0.889	0.891	0.854	0.875	0.878
SEE_{boot}[i]	0.209	0.222	0.206	0.228	0.237	0.217
r^2_{LHO}[j]	0.249	0.273	0.300	0.184	0.177	0.280
SD_{LHO}[k]	0.555	0.590	0.570	0.569	0.627	0.573
r^2_{5cv}[l]	0.423	0.431	0.455	0.361	0.452	0.463
SD_{5cv}[m]	0.515	0.552	0.538	0.530	0.553	0.523

[a] Correlation coefficient. [b] Standard error of estimate. [c] Ratio of r^2 explained to unexplained = $r^2/(1-r^2)$. [d] Cross-validated correlation coefficient after the leave-one-out procedure. [e] Standard error of prediction. [f] Predicted correlation coefficient for the test set of compounds. [g] Optimal number of principal components. [h] Average of correlation coefficient for 100 samplings using the bootstrapped procedure. [i] Average standard error of estimate for 100 samplings using the bootstrapped procedure. [j] Average cross-validated correlation coefficient for 50 runs using the leave-half-out (LHO) group. [k] Standard deviation of the average cross-validated correlation coefficient for 50 runs. [l] Average cross-validated correlation coefficient for 50 runs using five cross-validation groups. [m] Standard deviation of the average cross-validated correlation coefficient for 50 runs.

$(Y_{predicted} - Y_{observed})^2$ is the predictive residual sum of squares (PRESS).

The boot strapping analysis[37] for 100 runs and the number of cross-validations (e.g., two and five) were carried out and confirmed by the average value for 50 runs from each cross-validation. To test the utility of the model as a predictive tool, an external set of compounds with known activities but not used in model generation (the test set) was predicted. The predictive r^2, calculated by using eq 3, was based on molecules from the test set, and it was used to evaluate the predictive power of the CoMFA and CoMSIA models

$$\text{predictive } r^2 = 1 - (\text{“press”}/\text{SD}) \quad (3)$$

where SD is the sum of the squared deviations between the actual activities of the compounds in the test set and the mean activity of the compounds in the training set, and “press” is the sum of the squared deviations between predicted and actual activities for every compound in the test set. A predictive r^2 value of 1 signifies that the CoMFA model is perfectly predictive for the test set, while prediction of a mean value of the training set for every member in the test set yields a predictive $r^2 = 0$. The activity of the test set was predicted by the CoMFA and CoMSIA models using the predict command. CoMFA and CoMSIA coefficient maps were generated by interpolation of the pairwise products between the PLS coefficients and the standard deviations of the corresponding CoMFA or CoMSIA descriptor values.

RESULTS AND DISCUSSION

CoMFA Statistical Results. One of the major barriers in the 3D QSAR studies lies with the ‘congeners’, which misfit the final equation and are termed outliers. The reasons for the poor prediction may be their structural uniqueness, the insignificant mathematical value in defining the biological activity, or varied rates of metabolism. Exceptions are also observed in which experimentally observed parameters might be better than the calculated or vice versa; however, their inclusion in 3D QSAR studies at the cost of lower r^2_{cv} (cross-validated r^2) could be more baffling than helpful. Thus, the L1210, Molt 4/C8, and CEM training set was initially examined for outliers. Generally, if the residual of an inhibitor between the observed pIC_{50} and the predicted pIC_{50} values is approximately 1 logarithm unit, the inhibitor is considered as an outlier. In the L1210 CoMFA model, the residual values of compounds **9** and **17** were found to be 1.29 and 1.10, respectively; hence we decided to exclude these two compounds from the final L1210 CoMFA model. The underprediction of these two compounds could be explained by the sterically unfavorable yellow contour maps located in front of the plane of the 4-piperidone moiety by the *ortho*-NO_2 group of the B ring as discussed in the CoMFA and CoMSIA contour map analysis section. Exclusion of these two compounds led to an improvement in the r^2_{cv} value ($r^2_{cv} = 0.453$ for the 62 compound model and $r^2_{cv} = 0.485$ for the 60 compound model) in the L1210 CoMFA model. The Molt 4/C8 and CEM CoMFA models were generated using a training set of 62 compounds. The statistical results for the CoMFA model are summarized in Table 3. The predicted pIC_{50} values for cytotoxic potencies in the L1210, Molt 4/C8, and CEM cell lines training set compounds and the residual values are given in Tables 4−6, respectively. The corresponding graphs of the actual pIC_{50} versus the predicted pIC_{50} values for the training set by the CoMFA model are depicted in Figure 2A,C,E. For the L1210 training set, the CoMFA model gave an r^2_{cv} of 0.485 with five optimum numbers of components (ONC) and an r^2_{ncv} (non-cross-validated r^2) of 0.834 with an average absolute residual value of 0.19. For the Molt 4/C8 training set, the CoMFA model produced a r^2_{cv} of 0.532 (ONC = 5) and a r^2_{ncv} of 0.850 with an average absolute residual value of 0.21. For the CEM training set, the CoMFA model yielded r^2_{cv} of

Table 4. Observed and Predicted Activities for the Training Set for the L1210 Cell Line

		CoMFA		CoMSIA	
compd	obsd pIC_{50}	predicted	residual	predicted	residual
1	5.21	5.33	−0.12	5.03	0.18
2	5.60	5.23	0.37	5.17	0.43
3	5.36	5.25	0.11	5.18	0.18
4	5.78	5.67	0.11	5.59	0.19
5	5.10	5.25	−0.15	4.99	0.11
6	4.42	4.62	−0.20	4.75	−0.33
7	5.31	5.61	−0.30	5.50	−0.19
8	5.22	4.92	0.30	5.07	0.15
9[a]	5.73	4.44	1.29	5.57	0.16
10	4.84	4.92	−0.08	4.86	−0.02
11	4.92	5.10	−0.18	4.79	0.13
12	4.21	4.13	0.08	4.61	−0.40
13	4.35	4.51	−0.16	4.61	−0.26
14	4.41	4.48	−0.07	4.49	−0.08
15	4.34	4.43	−0.09	4.46	−0.12
16	4.30	4.20	0.10	4.47	−0.17
17[a]	5.19	4.09	1.10	5.13	0.06
18	4.40	4.23	0.17	4.57	−0.17
19	4.17	4.22	−0.05	4.12	0.05
20	4.56	4.33	0.23	4.56	0.00
21	5.71	5.70	0.01	5.59	0.12
22	5.48	5.55	−0.07	5.38	0.10
23	4.89	4.64	0.25	4.34	0.55
24	4.78	4.68	0.10	4.35	0.43
25	4.34	4.73	−0.39	4.59	−0.25
26	5.59	5.53	0.06	5.48	0.11
27	5.14	5.02	0.12	5.09	0.05
28	5.19	4.96	0.23	5.17	0.02
29	5.13	4.89	0.24	5.05	0.08
30	5.16	5.01	0.15	5.11	0.05
31	4.87	4.89	−0.02	4.98	−0.11
32	5.16	5.01	0.15	4.98	0.18
33	4.82	4.96	−0.14	5.05	−0.23
34	5.14	4.97	0.17	4.99	0.15
35	5.20	5.10	0.10	5.23	−0.03
36	4.74	4.95	−0.21	4.92	−0.18
37	5.02	4.89	0.13	5.05	−0.03
38	4.90	4.96	−0.06	5.09	−0.19
39	5.07	5.12	−0.05	5.31	−0.24
40	5.25	4.81	0.44	4.83	0.42
41	4.83	4.74	0.09	4.96	−0.13
42	4.94	4.73	0.21	4.72	0.22
43	3.77	3.92	−0.15	3.70	0.07
44	3.65	3.90	−0.25	3.73	−0.08
45	3.62	4.01	−0.39	3.99	−0.37
46	4.58	4.40	0.18	4.45	0.13
47	4.36	4.40	−0.04	4.22	0.14
48	4.40	4.42	−0.02	4.47	−0.07
49	4.89	4.61	0.28	4.95	−0.06
50[b]	4.40	4.60	−0.20	5.35	−0.95
51	5.58	5.82	−0.24	5.74	−0.16
52	4.85	4.64	0.21	4.92	−0.07
53	4.88	4.49	0.39	4.76	0.12
54	5.70	5.60	0.10	5.59	0.11
55	5.10	5.02	0.08	4.39	0.71
56	4.38	5.01	−0.63	4.52	−0.14
57	4.44	4.96	−0.52	4.54	−0.10
58	3.62	3.77	−0.15	3.95	−0.33
59	5.06	5.67	−0.61	5.46	−0.40
60	5.71	5.60	0.11	5.79	−0.08
61	5.82	5.93	−0.11	6.08	−0.26
62	6.38	5.98	0.40	6.11	0.27

[a] An outlier in the CoMFA model. [b] An outlier in the CoMSIA model.

Table 5. Observed and Predicted Activities for the Training Set for the Molt 4/C8 Cell Line

		CoMFA		CoMSIA	
compd	obsd pIC_{50}	predicted	residual	predicted	residual
1	5.27	5.68	−0.41	5.51	−0.24
2	5.61	5.42	0.19	5.35	0.26
3	5.77	5.57	0.20	5.46	0.31
4	5.84	5.94	−0.10	6.00	−0.16
5	5.79	5.54	0.23	5.45	0.34
6	5.06	4.98	0.08	5.09	−0.03
7	5.79	6.02	−0.23	5.99	−0.20
8	5.32	4.95	0.37	5.14	0.18
9	5.79	6.00	−0.21	5.74	0.05
10	5.18	5.07	0.11	5.23	−0.05
11	4.77	5.01	−0.24	5.07	−0.30
12	4.30	4.26	0.04	4.52	−0.22
13	4.41	4.77	−0.36	4.80	−0.39
14	4.85	4.70	0.15	4.67	0.18
15	4.44	4.54	−0.10	4.48	−0.04
16	4.48	4.39	0.09	4.61	−0.13
17	5.15	5.23	−0.08	5.05	0.10
18	4.47	4.48	−0.01	4.45	0.02
19	4.19	4.30	−0.11	4.61	−0.42
20	5.11	4.69	0.42	4.95	0.16
21	5.81	5.77	0.04	5.73	0.08
22	5.81	5.73	0.08	5.67	0.14
23	4.87	4.52	0.35	4.36	0.51
24	4.83	4.64	0.19	4.47	0.36
25	4.41	4.60	−0.19	4.70	−0.29
26	5.24	5.25	−0.01	5.39	−0.16
27	5.29	5.27	0.02	5.37	−0.08
28	5.31	5.19	0.12	5.28	0.03
29	5.28	5.12	0.16	5.20	0.08
30	5.38	5.22	0.16	5.28	0.10
31	5.26	5.18	0.08	5.27	−0.01
32	5.15	5.06	0.09	5.06	0.09
33	4.81	4.97	−0.16	4.96	−0.15
34	5.14	4.98	0.16	4.95	0.19
35	5.16	5.19	−0.03	5.33	−0.17
36	5.05	5.37	−0.32	5.36	−0.31
37	5.05	5.14	−0.09	5.18	−0.13
38	5.03	5.18	−0.15	5.12	−0.09
39	5.09	5.28	−0.19	5.21	−0.12
40	5.67	5.20	0.47	5.30	0.37
41	5.22	4.95	0.27	5.12	0.10
42	5.10	4.96	0.14	5.01	0.09
43	3.92	4.06	−0.14	3.69	0.23
44	3.63	4.06	−0.43	3.82	−0.19
45	3.76	4.29	−0.53	4.06	−0.30
46	4.40	4.27	0.13	4.20	0.20
47	4.42	4.27	0.15	4.09	0.33
48	4.38	4.41	−0.03	4.32	0.06
49	5.73	5.34	0.39	5.35	0.38
50	5.10	5.19	−0.09	5.23	−0.13
51	5.85	5.80	0.05	6.04	−0.19
52	5.54	5.28	0.26	5.38	0.16
53	5.09	4.96	0.13	4.92	0.17
54	5.82	5.58	0.24	6.59	−0.77
55	5.78	5.53	0.25	5.52	0.26
56	4.87	5.32	−0.45	5.33	−0.46
57	5.30	5.44	−0.14	5.47	−0.17
58	3.65	4.06	−0.41	4.50	−0.85
59	5.85	6.36	−0.51	6.28	−0.43
60	6.36	6.11	0.25	6.11	0.25
61	5.98	6.30	−0.32	6.33	−0.35
62	6.82	6.40	0.42	6.27	0.55

0.561 (ONC = 5) and r^2_{ncv} of 0.864 with an average absolute residual value of 0.18. Efforts were made to improve the r^2_{cv} values of all the models using different charges, alignment methods, steric/electrostatic cutoffs, and clogP as additional descriptors. Unfortunately all of these efforts led to lower r^2_{cv} values compared to those described in this manuscript (data not shown). Thus, we presume that these r^2_{cv} values were the best that could be obtained for these series of compounds. However, an $r^2_{cv} \geq 0.5$ is generally considered as an indication that the model is internally

Table 6. Observed and Predicted Activities for the Training Set for the CEM Cell Line

		CoMFA		CoMSIA	
compd	obsd pIC_{50}	predicted	residual	predicted	residual
1	5.61	5.70	−0.09	5.47	0.14
2	5.64	5.49	0.15	5.45	0.19
3	5.76	5.64	0.12	5.52	0.24
4	5.89	5.96	−0.07	6.01	−0.12
5	5.70	5.59	0.11	5.39	0.31
6	5.02	5.03	−0.01	5.01	0.01
7	5.78	5.95	−0.17	5.96	−0.18
8	5.21	4.88	0.33	5.05	0.16
9	5.86	6.05	−0.19	5.77	0.09
10	5.15	4.98	0.17	5.13	0.02
11	4.70	4.96	−0.24	5.03	−0.33
12	4.14	4.19	−0.05	4.46	−0.32
13	4.41	4.76	−0.35	4.78	−0.37
14	4.60	4.67	−0.07	4.62	−0.02
15	4.40	4.54	−0.14	4.46	−0.06
16	4.73	4.47	0.26	4.68	0.05
17	5.23	5.29	−0.06	5.15	0.08
18	4.59	4.60	−0.01	4.60	−0.01
19	4.30	4.32	−0.02	4.64	−0.34
20	5.09	4.70	0.39	5.05	0.04
21	5.77	5.75	0.02	5.72	0.05
22	5.81	5.76	0.05	5.70	0.11
23	4.84	4.58	0.26	4.35	0.49
24	4.80	4.69	0.11	4.53	0.27
25	4.59	4.69	−0.10	4.73	−0.14
26	5.41	5.40	0.01	5.53	−0.12
27	5.24	5.33	−0.09	5.39	−0.15
28	5.57	5.28	0.29	5.45	0.12
29	5.37	5.20	0.17	5.26	0.11
30	5.25	5.20	0.05	5.22	0.03
31	5.16	5.25	−0.09	5.25	−0.09
32	5.36	5.25	0.11	5.22	0.14
33	5.09	5.19	−0.10	5.29	−0.20
34	5.25	5.09	0.16	5.04	0.21
35	5.23	5.25	−0.02	5.38	−0.15
36	5.06	5.40	−0.34	5.32	−0.26
37	5.02	5.22	−0.20	5.29	−0.27
38	5.05	5.29	−0.24	5.21	−0.16
39	5.09	5.27	−0.18	5.17	−0.08
40	5.33	5.21	0.12	5.25	0.08
41	5.55	5.02	0.53	5.23	0.32
42	5.12	4.91	0.21	4.94	0.18
43	3.95	4.08	−0.13	3.69	0.26
44	3.74	3.98	−0.24	3.78	−0.04
45	3.73	4.33	−0.60	4.14	−0.41
46	4.82	4.63	0.19	4.59	0.23
47	4.44	4.49	−0.05	4.31	0.13
48	4.75	4.77	−0.02	4.67	0.08
49	5.64	5.25	0.39	5.27	0.37
50	5.05	5.10	−0.05	5.14	−0.09
51	5.79	6.04	−0.25	5.96	−0.17
52	5.15	5.07	0.08	5.19	−0.04
53	5.02	4.75	0.27	4.76	0.26
54	5.82	5.61	0.21	5.48	0.34
55	5.77	5.60	0.17	5.56	0.21
56	5.06	5.43	−0.37	5.52	−0.46
57	5.69	5.55	0.14	5.61	0.08
58	3.79	4.10	−0.31	4.54	−0.75
59	5.83	6.28	−0.45	6.16	−0.33
60	6.31	6.09	0.22	6.15	0.16
61	5.97	6.29	−0.32	6.35	−0.38
62	6.59	6.26	0.33	6.13	0.46

predictive, and thus the r^2_{cv} values obtained in the present study imparted reliability to our CoMFA models.

To further evaluate the robustness and statistical confidence of the derived models, bootstrapping[35] analysis for 100 runs was performed (Table 3). Bootstrapping involves the generation of many new data sets from the original data sets after randomly choosing samples from the original data set. Subsequently a cross-validation analysis was applied to the set of compounds in the training set to investigate the stability of the CoMFA models. The training set models were also cross-validated using two (Leave-Half-Out) and five (Leave 20% out) cross-validation groups 50 times each. The average and standard deviation values of cross-validation r^2 are shown in Table 3.

The predictive abilities of the CoMFA models were determined using a set of 16 test compounds (15 test compounds were used for the L1210 assay) not included in the model generation. The detailed experimental and predicted pIC_{50} values for cytotoxic potencies toward the L1210, Molt 4/C8, and CEM cell lines test set compounds are listed in Tables 7−9, respectively. The corresponding graphs of the actual pIC_{50} versus the predicted pIC_{50} values for the test set by CoMFA model are depicted in Figure 2A,C,E. The predicted r^2 values from the CoMFA model were found to be 0.591, 0.729, and 0.666 using L1210, Molt 4/C8, and CEM cells, respectively (Table 3). Compound **77** from the L1210 CoMFA test set was omitted since it was poorly predicted. Unlike most active compounds **60**−**62** from the 4-piperidone series, compound **77** of the test set lacks the essential *N*-acryloyl group. The overprediction of compound **77** can be explained based on the presence of the electron withdrawing $-NO_2$ group at the *para* position of the A and B rings. Given that the actual pIC_{50} values of the compounds within each test set against the appropriate cell line fluctuate within a range of approximately 3 log units, the fact that all three CoMFA models predicted the cytotoxic potencies of all the test set compounds within 1 log unit from the experimentally determined value further verified the predictability of these models.

CoMSIA Statistical Results. Three CoMSIA models, one for each cell line, were generated from the training set of 62 compounds, except in the case of the L1210 CoMSIA model we used 61 compounds. Compound **50** was found to be an outlier in the L1210 CoMSIA model. An overprediction of this compound could be due to the more electropositive potential in the A and B rings which are surrounded by a blue contour map as discussed in the CoMFA and CoMSIA contour map section. A summary of the statistical results associated with these models is shown in Table 3. It has been established that the five different descriptor fields are not totally independent of each other and that such dependencies on individual fields usually decrease the statistical significance of the CoMSIA models.[38,39] An evaluation of which one of the five CoMSIA fields are actually needed for the generation of a predictive model was performed by computing all possible combinations of fields (Supporting Information, Tables S1−S3). The steric and hydrophobic fields yielded the best individual field models with r^2_{cv} of (0.317 and 0.414), (0.503 and 0.496), and (0.526 and 0.497) for the L1210, Molt 4/C8, and CEM cell lines, respectively. Employing the donor or acceptor fields produced the lowest internal predictivity. In the combined models, the highest r^2_{cv} was obtained by combining the steric, electrostatic, hydrophobic, and H-bond donor fields ($r^2_{cv} = 0.513$ and $r^2_{ncv} = 0.833$) for the L1210 assay. For the Molt 4/C8 and CEM cells, the best CoMSIA models were obtained by the combination of steric, electrostatic, and hydrophobic fields yielding $r^2_{cv} = 0.531$ and $r^2_{ncv} = 0.828$ for Molt 4/C8 and

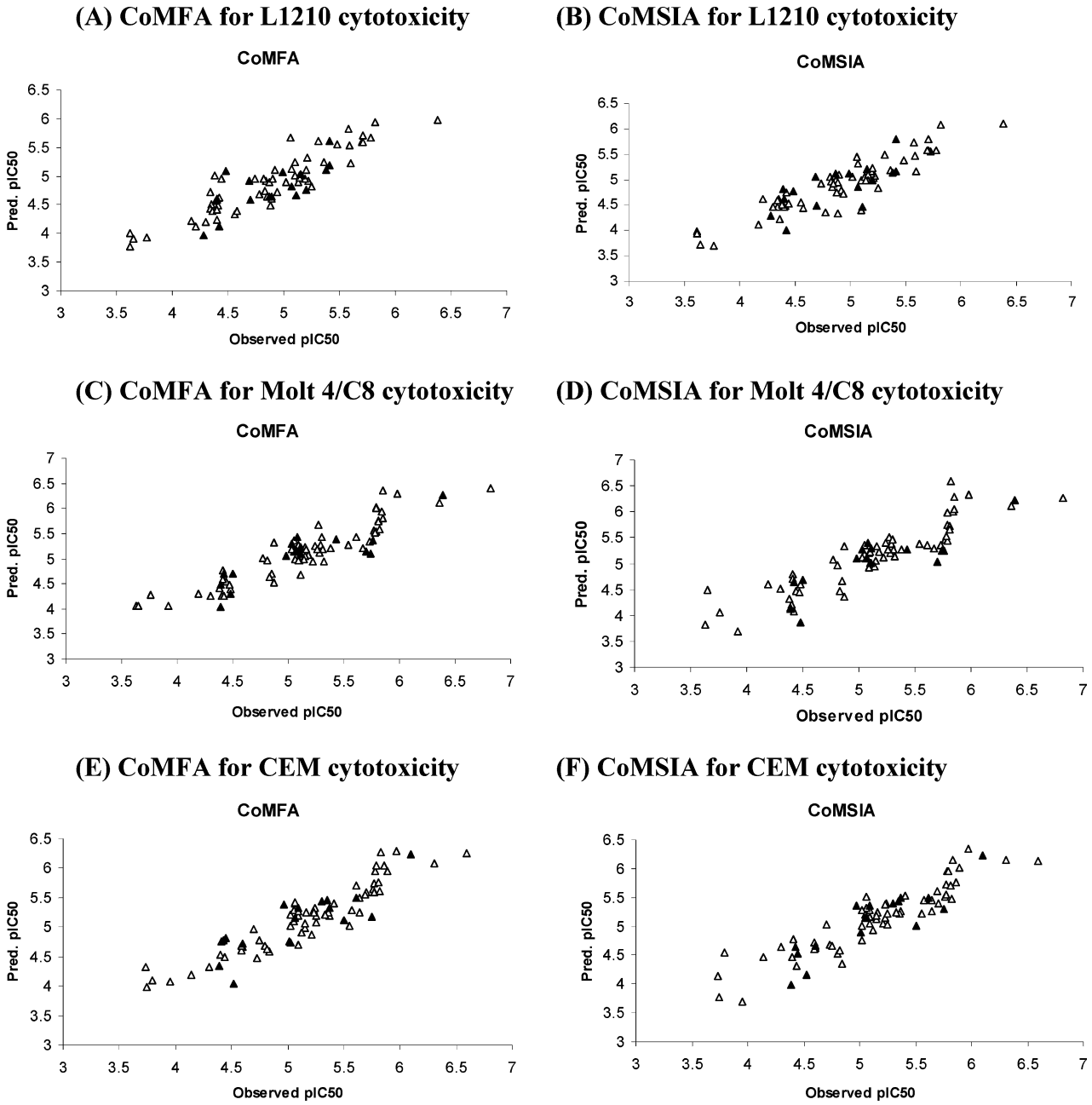

Figure 2. CoMFA and CoMSIA predictions for the training (△) and test (▲) sets for cytotoxic activities.

$r^2_{cv} = 0.560$ and $r^2_{ncv} = 0.841$ for CEM. As discussed in the CoMFA statistical results section, the use of different charges, alignment methods, steric/electrostatic cutoffs, and clogP as additional descriptors led to lower r^2_{cv} values than those generated for the final models. The detailed experimental and predicted pIC_{50} values based on the selected CoMSIA model for the training set are shown in Tables 4−6. The corresponding graphs of the actual pIC_{50} versus the predicted pIC_{50} values for the training set by CoMSIA model are shown in Figure 2B,D,F. The resulting CoMSIA models were further subjected to bootstrapping analysis and cross-validations using the leave-group-out technique to assess the robustness and statistical confidence of the derived models as described in the CoMFA statistical results (Table 3). The predictive abilities of CoMSIA models were determined from a set of 16 test compounds not included in the model generation. The detailed experimental and predicted pIC_{50} values for the cytotoxic potencies in the L1210, Molt 4/C8, and CEM CoMSIA test set compounds are listed in Tables 7−9, respectively. The corresponding graphs of the actual pIC_{50} versus the predicted pIC_{50} values for the test set by the CoMSIA model are depicted in Figure 2B,D,F. The predicted r^2 from the CoMSIA model were found to be 0.562, 0.652, and 0.729 for L1210, Molt 4/C8, and CEM cell lines, respectively (Table 3). The excellent predictability across a broad range of structurally diverse cytotoxic compounds suggests that these 3D QSAR models are valuable tools for guiding the rational design of potent cytotoxic compounds.

CoMFA and CoMSIA Contour Maps. For each cell line the contour maps for CoMFA and CoMSIA fields were produced and analyzed. These fields usually provide a more detailed understanding of the binding pockets of the macromolecular target, highlighting the key structural features required for the biological activity. In the CoMFA steric field, the green (sterically favorable) and yellow (sterically unfavorable) contours represent 80% and 20% level contributions,

Table 7. Observed and Predicted Activities for the Test Set Using L1210 Cells

		CoMFA		CoMSIA	
compd	obsd pIC_{50}	predicted	residual	predicted	residual
63	5.41	5.19	0.22	5.17	0.24
64	5.07	4.82	0.25	4.87	0.20
65	4.40	4.59	−0.19	4.62	−0.22
66	4.28	3.96	0.32	4.28	0.00
67	5.38	5.11	0.27	5.15	0.23
68	5.11	4.67	0.44	4.46	0.65
69	5.15	5.03	0.12	5.21	−0.06
70	4.99	5.07	−0.08	5.13	−0.14
71	4.69	4.91	−0.22	5.05	−0.36
72	5.20	4.76	0.44	4.98	0.22
73	4.42	4.12	0.30	4.01	0.41
74	4.70	4.59	0.11	4.48	0.22
75	4.87	4.65	0.22	5.12	−0.25
76	4.39	4.56	−0.17	4.81	−0.42
77[a]	4.48	5.09	−0.61	4.78	−0.30
78	5.41	5.62	−0.21	5.81	−0.40

[a] An outlier in the CoMFA model.

Table 8. Observed and Predicted Activities for the Test Set Using Molt 4/C8 Cells

		CoMFA		CoMSIA	
compd	obsd pIC_{50}	predicted	residual	predicted	residual
63	5.43	5.38	0.05	5.27	0.16
64	5.70	5.14	0.56	5.04	0.66
65	4.50	4.71	−0.21	4.69	−0.19
66	4.39	4.04	0.35	4.13	0.26
67	5.76	5.37	0.39	5.25	0.51
68	4.42	4.71	−0.29	4.65	−0.23
69	5.11	5.23	−0.12	5.30	−0.19
70	5.11	5.10	0.01	5.01	0.10
71	5.03	5.30	−0.27	5.28	−0.25
72	5.74	5.10	0.64	5.24	0.50
73	4.48	4.30	0.18	3.87	0.61
74	4.39	4.47	−0.08	4.14	0.25
75	5.07	5.16	−0.09	5.11	−0.04
76	4.98	5.05	−0.07	5.09	−0.11
77	5.08	5.43	−0.35	5.41	−0.33
78	6.39	6.26	0.13	6.23	0.16

Table 9. Observed and Predicted Activities for the Test Set Using CEM Cells

		CoMFA		CoMSIA	
compd	obsd pIC_{50}	predicted	residual	predicted	residual
63	5.30	5.44	−0.14	5.40	−0.10
64	5.50	5.12	0.38	5.01	0.49
65	4.60	4.72	−0.12	4.67	−0.07
66	4.52	4.04	0.48	4.16	0.36
67	5.61	5.50	0.11	5.50	0.11
68	4.43	4.77	−0.34	4.65	−0.22
69	5.37	5.32	0.05	5.49	−0.12
70	5.09	5.32	−0.23	5.35	−0.26
71	4.97	5.38	−0.41	5.35	−0.38
72	5.75	5.17	0.58	5.30	0.45
73	4.39	4.34	0.05	3.98	0.41
74	4.45	4.81	−0.36	4.52	−0.07
75	5.06	5.15	−0.09	5.17	−0.11
76	5.01	4.76	0.25	4.89	0.12
77	5.35	5.46	−0.11	5.43	−0.08
78	6.10	6.24	−0.14	6.22	−0.12

respectively. Similarly the red (negative charge favorable) and blue (positive charge favorable) contours in the CoMFA electrostatic field represent 80% and 20% level contributions, respectively. Since, for all three CoMSIA models, the combined contribution of electrostatic and hydrophobic descriptors is >60%, only these two types of fields are discussed further in detail. In the CoMSIA electrostatic field, the red (negative charge favorable) and blue (positive charge favorable) contours represent 80% and 20% level contributions, respectively. Similarly the white (hydrophobic favorable) and orange (hydrophobic unfavorable or hydrophilic favorable) contours represent 80% and 20% level contributions, respectively, in the CoMSIA hydrophobic field. To aid in the visualization of the CoMFA and CoMSIA fields, the most potent compound **62** was overlaid in the contour maps.

The L1210 CoMFA steric contour map is shown in Figure 3A. The *N*-acryloyl group falls into a sterically favorable green contour, suggesting that the steric bulk in this position is crucial for potent cytotoxic activity. This contour of favorable steric interaction remains unoccupied by compounds **55** (pIC_{50} = 5.10 M), **56** (pIC_{50} = 4.38 M), **57** (pIC_{50} = 4.44 M), and **58** (pIC_{50} = 3.62 M) owing to the lack of the N-substituent of the piperidine ring and appears to account for their reduced cytotoxic potencies. The most potent compounds **60** (pIC_{50} = 5.71 M), **61** (pIC_{50} = 5.82 M), and **62** (pIC_{50} = 6.38 M) possess the *N*-acryloyl group which seems to be playing an important role in their predominantly positive effect on cytotoxic potencies. The colocalization of the *N*-acryloyl group within the green (sterically favorable CoMFA field) and white (hydrophobic favorable CoMSIA field) contour maps suggests the importance of steric bulk and hydrophobicity at this position. The two green contour maps placed onto the *meta* and *para* positions of the A ring indicate that steric bulk at these positions is important for cytotoxic activity. These two green contour maps were found to be colocalized with the red contour map indicating a favorable effect of the steric bulk with high electron density containing groups such as $-OCH_3$. Two small green contour maps around the B ring suggest the sterically favorable region. Four yellow contour maps, three of them behind the plane of the 4-piperidone moiety and one being in front of the plane, indicate that occupancy of these sterically unfavorable maps which would have a negative effect on cytotoxic potencies. For example, the *tert*-butyl group at the 4-position of the cyclohexanone moiety in the least active compounds **43** (pIC_{50} = 3.77 M), **44** (pIC_{50} = 3.65 M), and **45** (pIC_{50} = 3.62 M) was found to be in contact with these yellow contour maps. This may be due to a collision between the *tert*-butyl group and one or more portions of an important binding site. A small yellow contour map near the *para* position of the B ring suggests that large substituents in this position would be unfavorable for cytotoxic activity. In addition, a small yellow contour map located near the methine hydrogen of the benzylidene moiety near (B ring) indicates that steric bulk in this region would decrease cytotoxic potency. The probable mechanism of the cytotoxic activity of the benzylidene derivatives is likely thiol alkylation as investigated previously in our laboratory. The localization of a small yellow contour near the reactive methine corroborates with this mechanism. Thus, the L1210 CoMFA steric contours explain the differences in the overall cytotoxic properties of the compounds due to differences in spatial arrangements.

Figure 3B reveals the electrostatic contour maps for the CoMFA analysis of L1210 cytotoxic activity. The large blue contour maps wrapped around the A and B rings indicate

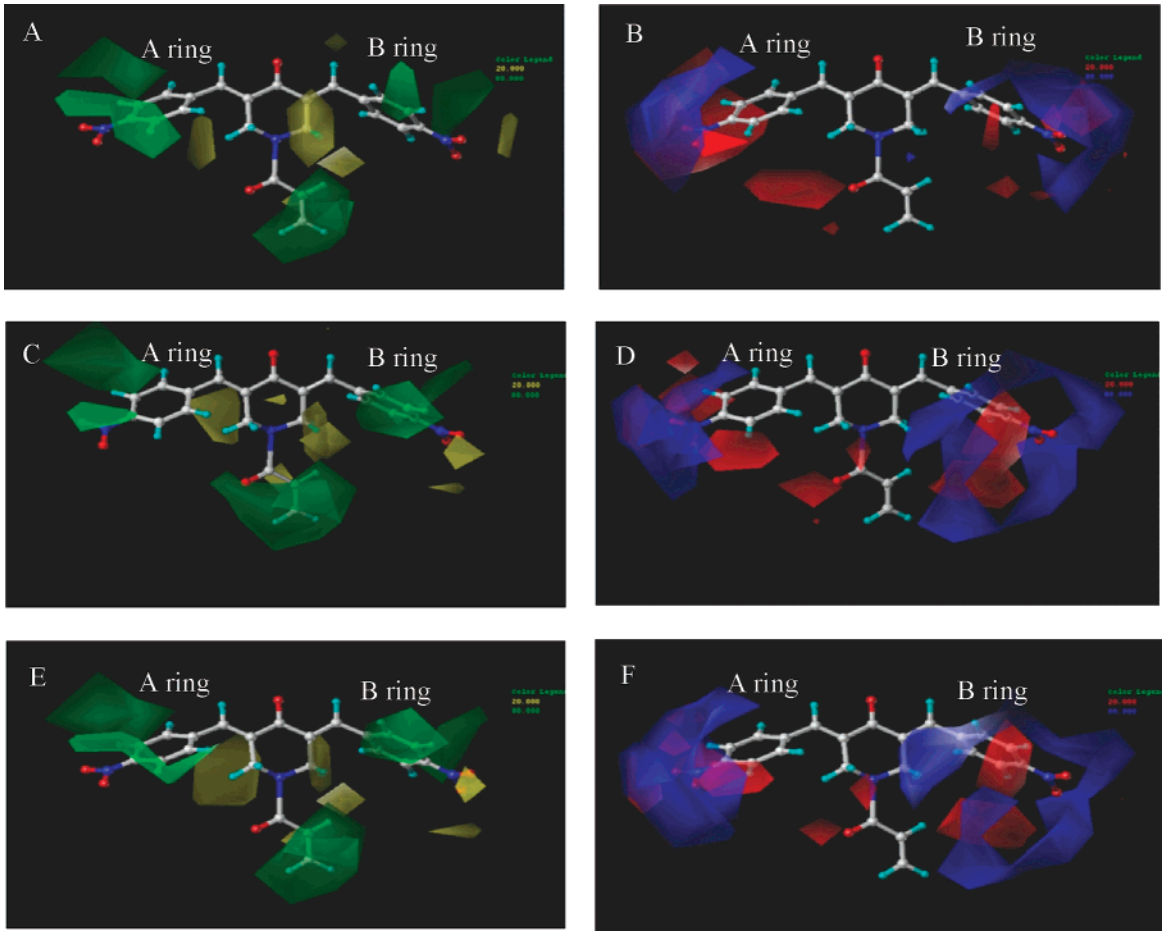

Figure 3. CoMFA contour maps are shown in the presence of the most potent compound **62**. (A) Steric fields generated with the CoMFA model based on L1210 cytotoxic activity: green indicates regions where bulky groups increase activity, whereas yellow indicates regions where bulky groups decrease activity. (B) Electrostatic fields generated with the CoMFA model based on L1210 cytotoxic activity: blue indicates regions where more positively charged groups increase activity, whereas red indicates regions where more negatively charged groups increase activity. (C) Steric fields generated with the CoMFA model based on Molt 4/C8 cytotoxic activity: the color scheme is the same as in panel A. (D) Electrostatic fields generated with the CoMFA model based on Molt 4/C8 cytotoxic activity: the color scheme is the same as in panel B. (E) Steric fields generated with the CoMFA model based on CEM cytotoxic activity: the color scheme is the same as in panel A. (F) Electrostatic fields generated with the CoMFA model based on CEM cytotoxic activity: the color scheme is the same as in panel B.

that the electropositive potential in these rings increases cytotoxic potencies. The *para*-NO_2 (electron withdrawing) group on the benzylidene moiety depletes the electron density in the benzylidene ring, thus making the electrostatic potential more positive and thereby leading to compounds with enhanced cytotoxic potencies. One of the least active compounds **58** (pIC_{50} = 3.62 M) carries a $-N(CH_3)_2$ (electron donating) substituent at the *para* position of the B ring which is in contrast to that of the potent compounds carrying electron withdrawing groups in the corresponding position. The most potent compounds **60**−**62** possess electron withdrawing groups which helps to make the electrostatic potential of the A and B rings more positive. The red contour maps around the *meta* positions of the A ring indicate that electronegative groups at these positions would increase cytotoxic potency. Compound **4** with a *meta*-F (electronegative) substituent is more potent than compound **1** with a corresponding *meta*-H (electropositive) substituent on the benzylidene ring. For example, compound **7** with an electron donating $-OCH_3$ group at the *meta* position exhibits higher activity than compounds **10** and **11** having an electron withdrawing $-NO_2$ group at the *meta* position. The most active compound from the **27**−**53** series was compound **51** (pIC_{50} = 5.58 M) which has the *meta*-OCH_3 (electronegative) group, while the rest of the compounds from this series lack such a functional group. Another red contour map located near the carbonyl oxygen of the *N*-acryloyl moiety explains the importance of the electronegative group for potent cytotoxic activity. The most potent compounds from the entire series are compounds **60**−**62** whose carbonyl oxygen (electronegative) atom touches this red contour map. Several small red contour maps around the B ring suggest the importance of electronegative groups at the *meta* position of the B ring for the potent cytotoxic activity.

The L1210 CoMSIA electrostatic contour map for cytotoxic activity is depicted in Figure 4A. The small and large blue contour maps were located on the *para* positions of the A and B rings, respectively. This finding indicated that the simultaneous presence of electron withdrawing groups at the *para* positions of the A and B rings is essential for potent cytotoxic activity. Two small red contour maps located on the *meta* position of the A ring suggest the importance of the electronegative group for potent cytotoxic activity.

The hydrophobic contour map of the CoMSIA model based on L1210 cytotoxic activity is displayed in Figure 4B. The white contour map located on the *meta* and the *para*

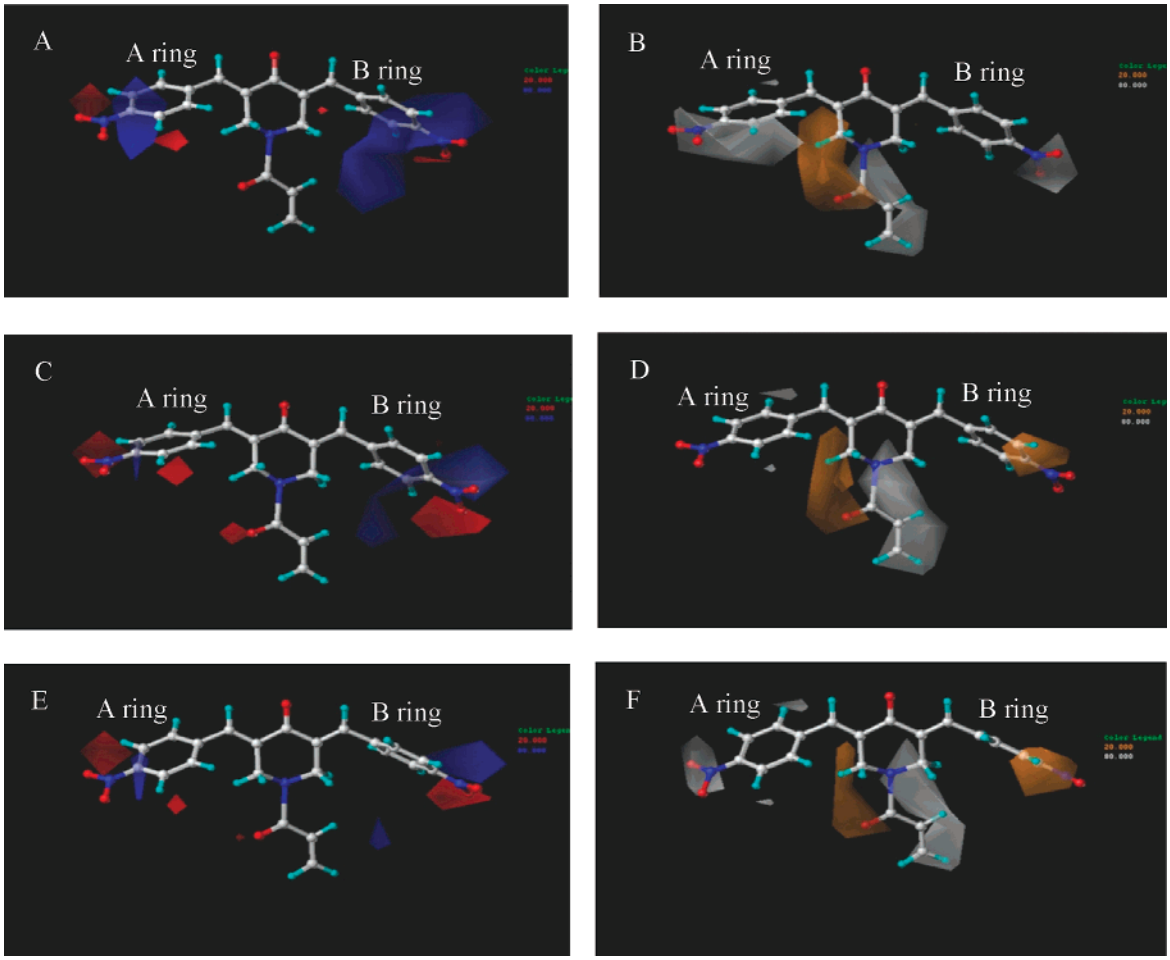

Figure 4. CoMSIA contour maps are shown in the presence of the most potent compound **62**. **(**A) Electrostatic fields generated with the CoMSIA model based on L1210 cytotoxic activity: blue indicates regions where more positively charged groups increase activity, whereas red indicates regions where more negatively charged groups increase activity. (B) Hydrophobic fields generated with the CoMSIA model based on L1210 cytotoxic activity: white (hydrophobic-favorable) and orange (hydrophobic-unfavorable). (C) Electrostatic fields generated with the CoMSIA model based on Molt 4/C8 cytotoxic activity: the color scheme is the same as in panel A. (D) Hydrophobic fields generated with the CoMSIA model based on Molt 4/C8 cytotoxic activity: the color scheme is the same as in panel B. (E) Electrostatic fields generated with the CoMSIA model based on CEM cytotoxic activity: the color scheme is the same as in panel A. (F) Hydrophobic fields generated with the CoMSIA model based on CEM cytotoxic activity: the color scheme is the same as in panel B.

positions of the A ring suggest that hydrophobic groups at these positions would increase the cytotoxic activity. Thus the marked potencies of **60** and **61** may have been due, inter alia, to the hydrophobicity imparted by the chloro atoms ($\pi = 0.71$ for each chloro substituent). Another small white contour map falls at the *para* substituent of the B ring indicating that small hydrophobic groups such as −Cl and −F at this position would be favorable for cytotoxic activity. The *N*-acryloyl group in compounds **60**−**62** fits well into the white contour map which is favorable for hydrophobic groups. Even though compounds **43**−**45** possess the hydrophobic-favorable *tert*-butyl group at the C_4 position of the cyclohexanone moiety, they exhibit low cytotoxic potencies as their *tert*-butyl group is located away from this white contour. The large orange contour map located behind the plane of the 4-piperidone ring suggests that occupancy of this field by a hydrophobic group would be detrimental for cytotoxic activity as exemplified by the poorly active compounds **43**−**45**. However, occupancy of this contour map by relatively less hydrophobic groups would enhance the cytotoxic activity as exemplified by reasonably high cytotoxic activity of compounds **46**−**48** with a C_4 carboethoxymethylene substituent, compounds **49**−**51** with a C_4 dimethylenedioxy substituent, and compounds **52**−**53** with a C_4 acetoxy substituent compared to compounds **43**−**45** having a corresponding C_4 *tert*-butyl substituent.

The steric contours of the CoMFA analysis for Molt 4/C8 cytotoxic activity are shown in Figure 3C. The *N*-acryloyl moiety fits well into a sterically favorable large green contour map similar to that seen in the L1210 CoMFA steric model. For example, the most potent compounds **59**−**62** possess a bulky *N*-acryloyl group within this region. As in the L1210 CoMFA model, the least active compounds **43**−**45** orient their bulky *tert*-butyl group away from the large central green contour and approach the sterically unfavorable four yellow contour maps behind the plane of the cyclohexanone ring. Each of the methyl substituents of the *tert*-butyl group partially touches the four yellow contour maps. One medium size sterically unfavorable yellow contour was seen on the front side of the plane of the 4-piperidone ring (precisely around the C_2 position of the 4-piperidone and the C_3 position of the cyclohexanone rings). These yellow contour maps together suggest the steric restrictions above and below the plane of the 4-piperidone, cyclohexanone, and 3,4-dihydro-

1*H*-naphthalen-2-one rings. Two small yellow contour maps in the vicinity of the *para* substituent of the B ring indicate that bulky steric groups are unfavorable at this position. The *para*-$N(CH_3)_2$ group on the B ring of the poorly active compounds **12** (pIC_{50} = 4.30 M) and **58** (pIC_{50} = 3.65 M) touches these two yellow contour maps. The sterically favorable large and small green contour maps were seen at the *meta* and the *para* positions, respectively, of the A ring. Among compounds **3**−**5**, compound **4** with the *meta*-fluoro substituent on the A ring is the most potent as it occupies the sterically favorable green contour map. The reasonably good potency of compound **35** (pIC_{50} = 5.16 M) could be due to the occupancy of its *meta*-dimethylaminomethyl group by a large green contour on the *meta* position of the A ring. A sterically favorable green contour map in the vicinity of the *ortho* and the *meta* positions of the B ring may have resulted due to the slightly different plane of the benzylidene ring in the case of the most potent compounds **59**−**62**. A small green contour was observed around the second *meta* position of the B ring resulting from the corresponding piperidinylmethyl substituents in the moderately cytotoxic compounds **32** (pIC_{50} = 5.15 M), **33** (pIC_{50} = 4.81 M), and **34** (pIC_{50} = 5.14 M).

The electrostatic contour maps constructed on the basis of the CoMFA analysis for Molt 4/C8 cytotoxic activity are shown in Figure 3D. The large blue contour maps at the *para* position of the A and B rings suggest the importance of electropositive groups for cytotoxic activity. It was interesting to note that the blue contour map on the B ring is larger encompassing the entire B ring. This observation was not surprising since most of the highly active compounds were found to possess electron withdrawing substituents such as −Cl, F, $-NO_2$ or −COOH on the benzylidene moiety. These electron withdrawing groups deplete the electron density in the benzylidene ring, thus making the electrostatic potential more positive and thereby leading to compounds with enhanced cytotoxic activity. Several red contour maps were noticed around the *meta* positions of the A and B rings which indicate that electronegative groups at these positions would increase the cytotoxic activity. For example, among compounds **27**−**53**, compound **51** (pIC_{50} = 5.85 M) was the most potent cytotoxic agent which could be the result of localization of its *meta*-methoxy groups within these red contour maps. The red contour map located on the carbonyl oxygen of the *N*-acryloyl group highlights the importance of an electronegative group for the potent cytotoxic activity of compounds **59**−**62**.

The Molt 4/C8 cytotoxicity CoMSIA electrostatic contour map is shown in Figure 4C. Unlike the L1210 CoMSIA model, a small blue contour map at the *para* position of the A ring implies that the presence of an electron withdrawing group would increase the cytotoxic activity. The small size of this contour suggests a minor role played by this contour in explaining the variation in cytotoxic potencies. The relatively large blue contour at the *para* position passing through the B ring was quite similar to that seen in the CoMFA electrostatic fields which indicate that an electropositive potential in this ring would increase cytotoxic properties. Two small red contour maps located at the *meta* positions of the A ring indicated the presence of electronegative groups would increase the cytotoxic potencies. Usually these positions are occupied by electron rich substituents such as −OH, $-OCH_3$, Cl, or −F in most of the highly active compounds **4** (pIC_{50} = 5.84 M), **7** (pIC_{50} = 5.79 M), **21** (pIC_{50} = 5.81 M), **51** (pIC_{50} = 5.85 M), and **61** (pIC_{50} = 5.98 M). A small red contour map around the carbonyl oxygen of *N*-acryloyl group was seen similar to that of CoMFA electrostatic fields. A red contour map in the vicinity of the *meta* position of ring B and the most electron rich oxygen atom of the $-NO_2$ group at the *para* position of ring B indicate the presence of an electronegative group in this region should increase the cytotoxic activity.

The hydrophobic contour map of the CoMSIA model based on the Molt 4/C8 cytotoxic activity is displayed in Figure 4D. The hydrophobic contour maps of the Molt 4/C8 were similar to that seen in the L1210 CoMSIA model. However, we noticed a few variations in the contour size and/or the appearance of new contours. In contrast to the L1210 CoMSIA model, the Molt 4/C8 data showed an orange contour map at the *para* position of the B ring, which suggests that hydrophilic groups at this position would be more favorable for Molt 4/C8 cytotoxic activity than they would be for L1210 cytotoxic activity. Most of the highly active compounds usually carry heteroatoms at this position which could provide a hydrophilic environment around this region due to the involvement of potential hydrogen bonding interactions with polar groups on the receptor. In addition, the absence of a significant white contour on the A ring suggests that hydrophobic groups are not required for the cytotoxic activity using Molt 4/C8 cell lines. However, we observed a new small white contour around the *ortho* position of the A ring, which implies the presence of hydrophobic group at this position would increase cytotoxic potencies. The potent cytotoxic activity of compound **54** (pIC_{50} = 5.82 M) could be due to the occupancy of this white contour by the *ortho*-NO_2 group of the A ring. Additional support for the potent cytotoxic activity of compounds **59**−**62** could be due to the closeness between the *N*-acryloyl oxygen atom and the hydrophobic unfavorable (hydrophilic favorable) orange contour map.

The CEM CoMFA steric contour map is shown in Figure 3E. The sterically favorable green contour maps on the A and B rings and a large green contour map on the *N*-acryloyl group were found to be similar to that of the L1210 CoMFA model. As shown in Figure 3F, the electrostatic contour maps for the CoMFA analysis of CEM cytotoxic activity were quite similar to that of the Molt 4/C8 CoMFA model.

The CEM cytotoxic activity CoMSIA electrostatic contour map is depicted in Figure 4E. The large red contour on one of the *meta* positions of the A ring and the small red contour on another *meta* position of the same ring are similar to that of the Molt 4/C8 CoMSIA model except in size. A tiny red contour was observed near the carbonyl oxygen of the *N*-acryloyl group. A relatively small blue contour map was seen at the *para* position of the B ring (this contour was larger in the case of the Molt 4/C8 CoMSIA model). A red contour was also seen near the oxygen atom of the $-NO_2$ group on the B ring.

The hydrophobic contour map of the CoMSIA model based on CEM cytotoxic potencies is displayed in Figure 4F. A relatively small white contour map compared to the L1210 CoMSIA model was seen at the *para* position of the A ring (the corresponding white contour was missing in the case of the Molt 4/C8 CoMSIA model). A hydrophilic

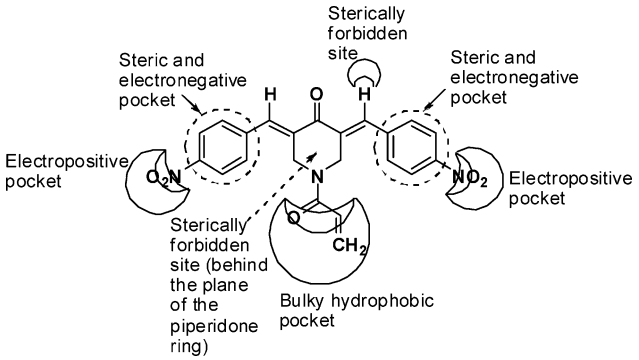

Figure 5. Proposed hypothetical receptor active site model for the bis(benzylidene) class of cytotoxic compounds.

favorable orange contour map was located at the *para* position of the B ring similar to that of the Molt 4/C8 CoMSIA model, while this field was replaced by the white contour in the case of the L1210 CoMSIA model. The rest of the fields were found to be similar to those described in the other two cell lines.

In summary, the CoMFA steric/electrostatic and CoMSIA electrostatic/hydrophobic contour maps associated with differences in the cytotoxic potencies demonstrate that the variations are dominated by structural features at the *meta* and the *para* positions of the A and B rings, the N-substituent of the 4-piperidone ring, and the C_4 substituent of the cyclohexanone ring. The common steric and electrostatic properties of the hypothetical receptor active site of all the cell lines for the bis(benzylidene) class of cytotoxic compounds are displayed in Figure 5. The presence of electron withdrawing groups at the *para*-position of the A and B rings and a bulky group, e.g., the acryloyl substituent, leads to potent cytotoxic activity toward the L1210, Molt 4/C8, and CEM cell lines. The central cyclic ring in the form of 4-piperidone seems optimal for potent cytotoxic activity in all of the tumor cell lines. Similarly a bulky group, e.g., a *tert*-butyl substituent present at the C_4-position of the central 1-cyclohexanone ring, was found to be detrimental for cytotoxic activity in all of the cell lines. The *N*,*N*-dimethylamino group at the *para*-position of A and B rings contributes to the lowering of cytotoxic potencies in all of the cell lines (e.g., compounds **12** and **58**). A monobenzylidene compound **66** from the test set also possesses a *N*,*N*-dimethylamino group at the *para*-position of the B ring which may account for its poor cytotoxic properties in all of the cell lines. The dimethylenedioxy substituent at the C_4 position of the cyclohexanone moiety may be important for the greater cytotoxic activity in the Molt 4/C8 and CEM cell lines as opposed to the L1210 cell line as exemplified by compounds **49**−**51** from the training set and compound **75** from the test set. It was observed that most of the monobenzylidene analogues were less potent compared to their dibenzylidene counterparts (e.g., compounds **13** vs **1** and **20** vs **7**), the former is due to the fact that important groups required for the potent cytotoxic properties are seen missing from the significant contour maps. For further confirmation, we attempted to align the B ring of compounds **13**−**20** and **23**−**25** onto the A ring of the template (compound **62**) as an alternative alignment strategy in order to check if there are any variations in the statistical data and contour maps, but we obtained similar results (data not shown). Unfavorable steric interactions between the C_8 proton of the 3,4-dihydro-1*H*-naphthalen-2-one ring and the *ortho* proton of the B ring in the 3,4-dihydro-1*H*-naphthalen-2-one series of compounds forces a change in the torsion angle ($\varphi \sim 135°$) defined by C_4 and C_5 as well as C_6 and the *ortho* carbon of the B ring compared to the corresponding torsion angle ($\varphi = 70°$) present in the template compound **62** which is a 4-piperidone analogue in which there is less steric hindrance. This observation is clearly visible in the alignment model (the B ring of the 3,4-dihydro-1*H*-naphthalen-2-one analogues distinctly exposes such a torsional change) as shown in Figure 1B. The only compound in a data set with a −C−C− single bond between the central cyclic ketone and the piperidine ring was compound **26**, which is thus amenable to more conformational freedom as well as steric bulk than the corresponding −C═C− containing compounds. This could be the reason why the piperidine ring of compound **26** fits well into the sterically favorable green contour map and as a result showed reasonably good cytotoxic activity. In addition, the electronegative nitrogen of the piperidine ring makes the rest of the carbons of the piperidine ring to be relatively more electropositive (a favorable phenomenon as suggested by the presence of the blue contour map) compared to the corresponding cyclohexyl ring.

CONCLUSION

A novel aspect in this study is the application of the CoMFA/CoMSIA method to the cytotoxic data of a diverse set of compounds tested toward L1210, Molt 4/C8, and CEM tumor cell lines. From these analyses, it is possible to predict the cytotoxic profile of newly designed compounds in each tumor cell line. A high bootstrapped r^2 value for all CoMFA and CoMSIA models with a small standard deviation indicates the existence of a similar relationship among all of the compounds used to build the model. In addition to steric and electrostatic fields, hydrophobic and hydrogen-bond donor fields are also important for cytotoxic activity. The predictive ability of the CoMFA model was best for the Molt 4/C8 cell line, while the CoMSIA model provided the best predictive ability for the CEM cell line. The 3D QSAR approach has revealed the importance of the shapes of different groups in influencing cytotoxic potencies to be determined. The excellent statistical correlations suggest that the 3D QSAR models are valuable computational tools for both the rational design of potent cytotoxic agents and the prediction of the cytotoxic property of these agents prior to their synthesis and bioevaluation. The syntheses of new cytotoxic compounds designed based on the 3D QSAR results are in progress.

ACKNOWLEDGMENT

Support from the start-up funds and resources provided by the College of Pharmacy and the Department of Pharmaceutical Sciences to T.T. at St. John's University are gratefully acknowledged. T.T. wishes to thank Drs. William Curtiss and Phillip Cruz at Tripos, Inc., for their excellent technical support. T.T. also wishes to thank Dr. Wayne Guida from the Moffitt Cancer Center and Research Institute for helpful discussions. Funds for the syntheses of the compounds were provided to J.R.D. by CoCensys Inc., U.S.A., Hoechst Marion Roussel Canada Research, and Purdue Pharma L. P., U,S,A.

Supporting Information Available: Results of combinations of different CoMSIA fields for each cell line (Tables S1−S3). This material is available free of charge via the Internet at http://pubs.acs.org.

REFERENCES AND NOTES

(1) Mutus, B.; Wagner, J. D.; Talpas, C. J.; Dimmock, J. R.; Phillips, O. A.; Reid, R. S. 1-*p*-Chlorophenyl-4,4-dimethyl-5-diethylamino-1-penten-3-one hydrobromide, a sulfhydryl-specific compound which reacts irreversibly with protein thiols but reversibly with small molecular weight thiols. *Anal. Biochem.* **1989**, *177*, 237−243.

(2) Baluja, G.; Municio, A. M.; Vega, S. Reactivity of some α,*β*-unsaturated ketones towards sulfhydryl compounds and their antifungal activity. *Chem. Ind*. **1964**, 2053−2054.

(3) Dimmock, J. R.; Raghavan, S. K.; Logan, B. M.; Bigam, G. E. Antileukemic evaluation of some Mannich bases derived from 2-arylidene-1,3-diketones. *Eur. J. Med. Chem.* **1983**, *18*, 248−254.

(4) Pati, H. N.; Das, U.; Sharma, R. K.; Dimmock, J. R. Cytotoxic thiol alkylators. *Mini-Rev. Med. Chem.* **2007**, *7*, 131−139.

(5) Benvenuto, J. A.; Connor, T. H.; Monteith, D. K.; Laidlaw, J. L.; Adams, S. C.; Matney, T. S.; Theiss, J. C. Degradation and inactivation of antitumor drugs. *J. Pharm. Sci*. **1993**, *82*, 988−991.

(6) Espinoza-Fonseca, L. M. The benefits of the multi-target approach in drug design and discovery. *Bioorg. Med. Chem.* **2006**, *14*, 896−897.

(7) Frantz, S. Playing dirty. *Nature* **2005**, *437*, 942−943.

(8) Galanski, M.; Keppler, B. K. Searching for the magic bullet: anticancer platinum drugs which can be accumulated or activated in the tumor tissue. *Anti-Cancer Agents Med. Chem.* **2007**, *7*, 55−73.

(9) Dimmock, J. R.; Arora, V. K.; Wonko, S. K.; Hamon, N. W.; Quail, J. W.; Jia, Z.; Warrington, R. C.; Fang, W. D.; Lee, J. S. 3,5-*bis*-Benzylidene-4-piperidones and related compounds with high activity towards P388 leukemia cells. *Drug Des. Delivery* **1990**, *6*, 183−194.

(10) Das, U.; Kawase, M.; Sakagami, H.; Ideo, A.; Shimada, J.; Molnár, J.; Baráth, Z.; Bata, Z.; Dimmock, J. R. 3-(3,4,5-Trimethoxyphenyl-1-oxo-2-propene: a novel pharmacophore displaying potent multidrug resistance reversal and selective toxicity. *Bioorg. Med. Chem.* **2007**, *15*, 3373−3380.

(11) Das, U.; Alcorn, J.; Shrivastav, A.; Sharma, R. K.; De Clercq, E.; Balzarini, J.; Dimmock, J. R. Design, synthesis and cytotoxic properties of novel 1-[4-(2-alkylaminoethoxy)phenylcarbonyl]-3,5-bis(arylidene)-4-piperidones and related compounds. *Eur. J. Med. Chem.* **2007**, *42*, 71−80.

(12) Das, U.; Gul, H. I.; Alcorn, J.; Shrivastav, A.; George, T.; Sharma, R. K.; Nienaber, K. H.; De Clercq, E.; Balzarini, J.; Kawase, M.; Kan, N.; Tanaka, T.; Tani, S.; Werbovetz, K. A.; Yakovich, A. J.; Manavathu, E. K.; Stables, J. P.; Dimmock, J. R. Cytotoxic 5-aryl-1-(4-nitrophenyl)-3-oxo-1,4-pentadienes mounted on alicyclic scaffolds. *Eur. J. Med. Chem.* **2006**, *41*, 577−585.

(13) Das, U.; Selvakumar, P.; Sharma, R. K.; Haas, T. A.; Dimmock, J. R. *N*-Acyl-3,5-bis(arylidene)-4-piperidones and related compounds which stimulate fyn kinase. *J. Enzyme Inhib. Med. Chem.* **2007**, *22*, 451−455.

(14) Jha, A.; Mukherjee, C.; Prasad, A. K.; Parmar, V. S.; De Clercq, E.; Balzarini, J.; Stables, J. P.; Manavathu, E. K.; Shrivastav, A.; Sharma, R. K.; Nienaber, K. H.; Zello, G. A.; Dimmock, J. R. *E*,*E*,*E*-1-(4-Arylamino-4-oxo-2-butenoyl)-3,5-bis(arylidene)-4-piperidones: a topographical study of some novel potent cytotoxins. *Bioorg. Med. Chem.* **2007**, *15*, 5854−5865.

(15) Dimmock, J. R.; Kumar, P.; Quail, J. W.; Pugazhenthi, U.; Yang, J.; Chen, M.; Reid, R. S.; Allen, T. M.; Kao, G. Y.; Cole, S. P. C.; Batist, G.; Balzarini, J.; De Clercq, E. Synthesis and cytotoxic evaluation of some styryl ketones and related compounds. *Eur. J. Med. Chem.* **1995**, *30*, 209−217.

(16) Dimmock, J. R.; Sidhu, K. K.; Chen, M.; Reid, R. S.; Allen, T. M.; Kao, G. Y.; Truitt, G. A. Evaluation of some Mannich bases of cycloalkanones and related compounds for cytotoxic activity. *Eur. J. Med. Chem.* **1993**, *28*, 313−322.

(17) Mitchell, J. B.; Russo, A. The role of glutathione in radiation and drug induced cytotoxicity. *Br. J. Cancer* **1987**, *55*, 96−104.

(18) Tsutsui, K.; Komuro, C.; Nishidai, T.; Shibamoto, Y.; Takahashi, M.; Abe, M. Chemosensitization by buthionine sulfoximine in vivo. *Int. J. Radiat. Oncol. Biol. Phys.* **1986**, *12*, 1183−1186.

(19) Dimmock, J. R.; Padmanilayam, M. P.; Zello, G. A.; Quail, J. W.; Oloo, E. O.; Prisciak, J. S.; Kraatz, H.-B.; Cherkasov, A.; Lee, J. S.; Allen, T. M.; Santos, C. L.; Manavathu, E. K.; De Clercq, E.; Balzarini, J.; Stables, J. P. Cytotoxic 1,3-diarylidene-2-tetralones and related compounds. *Eur. J. Med. Chem.* **2002**, *37*, 813−824.

(20) Dimmock, J. R.; Padmanilayam, M. P.; Zello, G. A.; Nienaber, K. H.; Allen, T. M.; Santos, C. L.; De Clercq, E.; Balzarini, J.; Manavathu, E. K.; Stables, J. P. Cytotoxic analogues of 2,6-bis(arylidene)-cyclohexanones. *Eur. J. Med. Chem.* **2003**, *38*, 169−177.

(21) Quinn, F. R.; Milne, G. W. A. Toxicities derived from anti-tumor screening data. *Fundam. Appl. Toxicol.* **1986**, *6*, 270−277.

(22) Dimmock, J. R.; Kumar, P.; Nazarali, A. J.; Motaganahalli, N. L.; Kowalchuk, T. P.; Beazely, M. A.; Quail, J. W.; Oloo, E. O.; Allen, T. M.; Szydlowski, J.; De Clercq, E.; Balzarini, J. Cytotoxic 2,6-bis-(arylidene)cyclohexanones and related compounds. *Eur. J. Med. Chem.* **2000**, *35*, 967−977.

(23) Dimmock, J. R.; Padmanilayam, M. P.; Puthucode, R. N.; Nazarali, A. J.; Motaganahalli, N. L.; Zello, G. A.; Quail, J. W.; Oloo, E. O.; Kraatz, H.-B.; Prisciak, J. S.; Allen, T. M.; Santos, C. L.; Balzarini, J.; De Clercq, E.; Manavathu, E. K. A Conformational and Structure-Activity Relationship Study of Cytotoxic 3,5-Bis(arylidene)-4-piperidones and Related *N*-Acryloyl Analogues. *J. Med. Chem.* **2001**, *44*, 586−593.

(24) Cramer, R. D.; III; Patterson, D. E.; Bunce, J. D. Comparative Molecular Field Analysis (CoMFA). 1. Effect of Shape on Binding of Steroids to Carrier Proteins. *J. Am. Chem. Soc.* **1988**, *110*, 5959−5967.

(25) Cramer, R. D., III; Bunce, J. D.; Patterson, D. E. Crossvalidation, Bootstrapping, and Partial Least Squares Compared with Multiple Regression in Conventional QSAR Studies. *Quant. Struct.-Act. Relat.* **1988**, *7*, 18−25.

(26) Klebe, G.; Abraham, U.; Mietzner, T. Molecular Similarity Indices in a Comparative Analysis (CoMSIA) of Drug Molecules to Correlate and Predict their Biological Activity. *J. Med. Chem.* **1994**, *37*, 4130−4146.

(27) *SYBYL 7.2*; Tripos Inc.: 1699 South Hanley Rd., St. Louis, MO 63144.

(28) Clark, M.; Cramer, R. D., III; Van Opdenbosch, N. Validation of the General-Purpose Tripos 5.2 Force Field. *J. Comput. Chem.* **1989**, *10*, 982−1012.

(29) Gasteiger, J.; Marsili, M. Iterative partial equalization of orbital electronegativity: A rapid access to atomic charges. *Tetrahedron* **1980**, *36*, 3219−3228.

(30) Patel, M. R.; Talele, T. T. 3D-QSAR studies on Malonyl Coenzyme A Decarboxylase Inhibitors. *Bioorg. Med. Chem.* **2007**, *15*, 4470−4481.

(31) Viswanadhan, V. N.; Ghose, A. K.; Revenkar, G. R.; Robins, R. K. Atomic physicochemical parameters for three-dimensional structure directed quantitative structure-activity relationships. 4. Additional parameters for hydrophobic and dispersive interactions and their application for an automated superposition of certain naturally occurring nucleoside antibiotics. *J. Chem. Inf. Comput. Sci.* **1989**, *29*, 163−172.

(32) Klebe, G. The use of composite crystal field environments in molecular recognition and the de novo design of protein ligands. *J. Mol. Biol.* **1994**, *237*, 212−235.

(33) Klebe, G.; Mietzner, T.; Weber, F. Methodological developments and strategies for a fast superposition of drug-size molecules. *J. Comput.-Aided Mol. Des.* **1999**, *13*, 35−49.

(34) Wold, S.; Albano, C.; Dunn, W. J.; Edlund, U.; Esbenson, K.; Geladi, P.; Hellberg, S.; Lindburg, W.; Sjostrom, M. In *Chemometrics: Mathematics and Statistics in Chemistry;* Kowalski, B., Ed.; Reidel: Dordrecht, The Netherlands, 1984; pp 17−95.

(35) Staahle, L.; Wold, S. Partial least squares analysis with cross-validation for the two-class problem: A Monte Carlo study. *J. Chemom.* **1987**, *1*, 185−196.

(36) Wold, S. Cross validatory estimation of the number of components in factor and principal components models. *Technometrics* **1978**, *4*, 397−405.

(37) Vong, R.; Geladi, P.; Wold, S.; Esbensen, K. Source contributions to ambient aerosol calculated by discriminant partial least squares regression (PLS). *J. Chemom.* **1988**, *2*, 281−296.

(38) Bringmann, G.; Rummey, C. 3D QSAR Investigations on antimalarial naphthylisoquinoline alkaloids by comparative molecular similarity indices analysis (CoMSIA), based on different alignment approaches. *J. Chem. Inf. Comput. Sci.* **2003**, *43*, 304−316.

(39) Bohm, M.; Strzebecher, J.; Klebe, G. Three-Dimensional Quantitative Structure-Activity Relationship Analyses using Comparative Molecular Field Analysis and Comparative Molecular Similarity Analysis to Elucidate Selectivity Differences of Inhibitors Binding to Trypsin, Thrombin, and Factor Xa. *J. Med. Chem.* **1999**, *42*, 458−477.

CI700210Z